Revista Brasileira de Ciências Ambientais
Brazilian Journal of Environmental Sciences

Application of Sentinel-2 Level-2A images for monitoring water surface in reservoirs in the semiarid region of Pernambuco—Brazil

Aplicação de imagens Sentinel-2 Nível 2A para monitoramento da superfície de água em reservatórios na região semiárida do estado de Pernambuco — Brasil

Jonas Felipe Santos de Souza[1], *Alfredo Ribeiro Neto*[1], *Santiago Peña-Luque*[2], *Marielle Gosset*[3]

ABSTRACT

Remote sensing techniques offer effective and efficient alternatives for observing the spatiotemporal dynamics of surface water in reservoirs. This paper aimed to analyze the applicability of Sentinel-2 Level-2A satellite images from 2016 to 2024 for mapping and monitoring the extent of water surfaces in reservoirs in the Sertão region of Pernambuco state. An automatic, unsupervised, and non-parametric algorithm was employed, combining water indices with reflectance bands of optical images to identify water pixels. The results were compared with two datasets: *in situ* monitoring and MapBiomas. Issues with optical images affected by clouds over the reservoir and errors in classifying water pixels were noted. Generally, the algorithm tended to underestimate the extent of the water surface due to difficulty detecting water pixels at the edges of the reservoirs. To mitigate this issue, an artificial neural network (ANN) was applied to correct the underestimation bias. The bias correction improved the performance of the metrics when the size and representativeness of the calibration sample were sufficient for training and building the ANN model.

Keywords: optical images; water indices; semiarid; artificial neural network.

RESUMO

As técnicas de sensoriamento remoto fornecem alternativas efetivas e eficientes para a observação da dinâmica espaçotemporal da água superficial em reservatórios. O objetivo deste artigo foi analisar a aplicabilidade de imagens do satélite Sentinel-2 de Nível 2A no período de 2016 a 2024 para o mapeamento e monitoramento da extensão da água superficial em reservatórios da região Sertão do estado de Pernambuco. Para tanto, foi utilizado um algoritmo automático não supervisionado e não paramétrico que faz a combinação de índices de água com bandas de reflectância de imagens ópticas para a identificação de *pixels* de água. Os resultados foram comparados com dois conjuntos de dados: monitoramento *in situ* e MapBiomas. Problemas com imagens ópticas afetadas por nuvens sobre o reservatório e erros de classificação dos *pixels* de água foram notados. Os resultados mostraram que, de modo geral, o algoritmo apresentou uma tendência de subestimação da extensão da superfície hídrica, decorrente da dificuldade de detecção dos *pixels* de água nas bordas dos reservatórios. Para atenuar esse comportamento, aplicou-se Rede Neural Artificial para corrigir o viés de subestimação. A correção de viés resultou em ganho de desempenho das métricas para os casos em que o tamanho e a representatividade da amostra de calibração foram suficientes para o treinamento e construção do modelo de Rede Neural Artificial.

Palavras-chave: imagens ópticas; índices de água; semiárido; rede neural artificial.

[1]Federal University of Pernambuco – Recife (PE), Brazil.

[2]Centre National d'Etudes Spatiales – Toulouse, France.

[3]Institut de Recherche pour le Développement, Géosciences Environment Toulouse – Toulouse, France.

Corresponding author: Jonas Felipe Santos de Souza – Universidade Federal de Pernambuco, Centro de Tecnologia, Departamento de Engenharia Civil e Ambiental – Avenida da Arquitetura, S/N – Cidade Universitária – CEP: 50740-530 – Recife (PE), Brazil. E-mail: jonas.ssouza@ufpe.br

Conflicts of interest: the authors declare no conflicts of interest.

Funding: This study was supported by Fundação de Amparo à Ciência e Tecnologia do Estado de Pernambuco (FACEPE). The second author would like to thank CNPq Productivity in Research (PQ).

Received on: 01/23/2024. Accepted on: 07/29/2024.

https://doi.org/10.5327/Z2176-94781927

Introduction

Water is essential for life in all its aspects. Historically, water-related ecosystems have provided ideal locations for human settlements, becoming the cradle of the first civilizations. Societies thrived alongside developing techniques for damming and storing surface water in lakes and reservoirs. These structures regulated water temporally and spatially, ensuring a continuous water supply throughout the annual hydrological cycle, even during dry periods. Additionally, reservoirs have been instrumental in flood control and, more recently, in energy generation (United Nations, 2018).

To mitigate the effects of prolonged droughts in the semiarid region of Northeast Brazil (NEB)—characterized mainly by intermittent rivers due to low soil water retention capacity and unfavorable climatic and meteorological conditions (Jardim et al., 2022; Marengo et al., 2017; 2022)—the government has promoted water storage policies since the late 19th century. These policies have focused on building and operating reservoirs, primarily in the nine states of NEB and the northern part of Minas Gerais state (Collischonn and Clarke, 2016).

Observations based on remote sensing data from the 1980s to 2000s have shown that approximately 29% of the total global land area has experienced reductions in biomass productivity. Of the total soil degradation area, around 9.2% of drylands are undergoing desertification (Bai et al., 2008). In the context of climate change, Pernambuco State, part of the NEB, is considered one of the most vulnerable states in Brazil. It faces extreme drought events in the Sertão and Agreste regions, with more than 135 municipalities in areas susceptible to desertification, putting over 2.6 million people at risk (Estado de Pernambuco, 2011). Given the critical role of water bodies in these regions, especially those used for water supply, monitoring water levels and the respective stored volume is crucial for understanding water availability.

Recognizing the limitations of existing *in situ* measurement networks in providing comprehensive knowledge on changes in water volume across various bodies of water (Chawla et al., 2020), remote sensing technology has emerged as a more effective and efficient method for observing surface water dynamics. This technology continuously monitors the Earth's surface at multiple scales (Huang et al., 2018). The increase in the number of satellites used in remote sensing today allows easy access to an extraordinary number of observations with high temporal and spatial resolution. Extracting information about the Earth's surface from images is based on an object's ability to reflect radiant energy within a specific spectrum. Surface water bodies can be accurately mapped by distinguishing the water spectrum from "non-water" spectra (Condeça et al., 2022). The global coverage of Sentinel-2 satellite observations has significantly improved the capabilities of optical sensor observation, offering higher spatial resolution (10 m) and a frequent revisit interval (5 days). Numerous studies have proposed and compared methods using radar data to extract water area extents. Most water detection methods fall into two categories, namely, image classification and threshold segmentation (Reis et al., 2021; Yilmaz et al., 2023).

Optical images are a vital component of passive remote sensing, which captures the spectrum of terrestrial objects by receiving reflected sunlight, primarily in the visible and infrared bands. Optical data are the primary sources used to extract information from water bodies (Li et al., 2022). Compared to other terrestrial objects, water has low reflectivity in the visible and near-infrared bands, a characteristic that forms the basis for mapping and extracting surface water (Huang et al., 2018). Among medium spatial resolution optical sensors, the Sentinel-2 satellite, operated by the European Space Agency (ESA) under the European Union's Copernicus Program, has been widely used for terrestrial observations, especially in hydrological and hydrodynamic studies (Drusch et al., 2012; Wieland and Martinis, 2020; Lasko et al., 2021; Filippucci et al., 2022). Sentinel-2 multispectral imagery is primarily used by applying spectral indices for water detection, such as the Normalized Difference Water Index (NDWI), Modified NDWI (MNDWI), Multi-Band Water Index (MBWI), and Automated Water Extraction Index (AWEI) (McFeeters, 1996; Xu, 2006; Feyisa et al., 2014; Wang et al., 2018). These indices typically require a calibration procedure for each acquisition date and coverage area, such as Otsu thresholding, which divides the index values in a bimodal histogram into "water" and "non-water" classes (Otsu, 1979). However, despite well-defined methods and data readings from optical sensors for water surface mapping, their use is limited by clouds and shadows that obscure surface observations.

Consequently, sensors can miss the maximum extent of water in lakes and reservoirs during flood events due to cloud cover, leading to data gaps and an inability to capture the precise magnitude of such events (Chawla et al., 2020; Li et al., 2022). One aspect that can help is the improved satellite revisit time, as the Sentinel-2 mission offers a frequency of 5 days near the equator. Therefore, applying these images in regions with high cloud incidence, such as the NEB, is essential.

This paper aimed to analyze the applicability of remote sensing using satellite images to map and monitor surface water extent in reservoirs. The study applied a water detection algorithm based on Sentinel-2 products to reservoirs in the Sertão region of Pernambuco, Brazil. Then, the accuracy of the surface water extent results was evaluated by comparing them with observed data. Finally, a method for bias correction of the water area data calculated using an artificial neural network (ANN) was proposed.

Materials and Methods

Study area

Three reservoirs were selected in the Sertão region of the Pernambuco state, NEB. The main selection criterion was the existence of *in situ* monitoring carried out by the National Water Agency (ANA). Table 1 presents the main characteristics of the reservoirs. The maxi-

mum surface area varies between 26.60 and 53.34 km^2. Figure 1 shows the study area location. The primary water use is human supply, with a withdrawal equivalent to 7.65 m^3.s^{-1} from these water bodies for distribution to several cities of the region (SEINFRA-PE, 2022).

Sentinel-2 data

Different processing procedures were developed to generate the Sentinel-2 Level-2A products, which provide images corrected for atmospheric conditions, such as clouds, cloud shadows, and surface reflectance. A necessary sub-product of this process is pixel classification, which generates masks for clouds, shadows, soil, and water. For water detection, products with lower than 20% cloud cover were selected from the Sentinel-2 Level-2A satellite data, covering the period from January 1, 2016, to June 30, 2024. These data were processed by the Sen2Cor processor (Mueller-Wilm et al., 2016) and acquired from the ESA-EC Copernicus Open Access Hub database (https://dataspace.copernicus.eu/).

Table 1 – Reservoir characteristics.

Reservoir	Maximum superficial area (km^2)	Maximum capacity (× 10^6 m^3)	River
Chapéu	26.60	187.69	Brígida
Serrinha II	44.23	311.08	Pajeú
Poço da Cruz	53.34	483.72	Moxotó

Comparison database

Two datasets were used to evaluate the estimated area extension. The first dataset comprises *in situ* monitoring data obtained from ANA's Reservoir Monitoring System (https://www.ana.gov.br/sar/). This dataset provides information on the reservoirs' water levels and the elevation-area-volume (EAV) curve, enabling the estimation of the water surface extent and stored volume. The results were validated by comparing the *in situ* water area values with those derived from the satellite images.

The second dataset consists of the surface water area from MapBiomas Collection 8, an initiative of the Climate Observatory's Greenhouse Gas Emissions Estimation System (SEEG/OC). This dataset, produced by a collaborative network of universities, technology companies, and NGOs, was launched in 2015. The initiative aimed to develop a low-cost method for creating an annual time series of land cover and use in Brazil using Landsat images processed by the Google Earth Engine (GEE) platform with a spatial resolution of 30 m, covering the period from 1985 to 2023 (Souza et al., 2020; SEEG/OC, 2022).

Water detection method

The WaterDetect algorithm, developed by Cordeiro et al. (2021), was used for water detection. This algorithm is automatic, unsupervised, and non-parametric, designed to identify water pixels in large areas from a single image obtained by optical sensors from the Sentinel-2 and Landsat 8 missions. WaterDetect employs automatic image

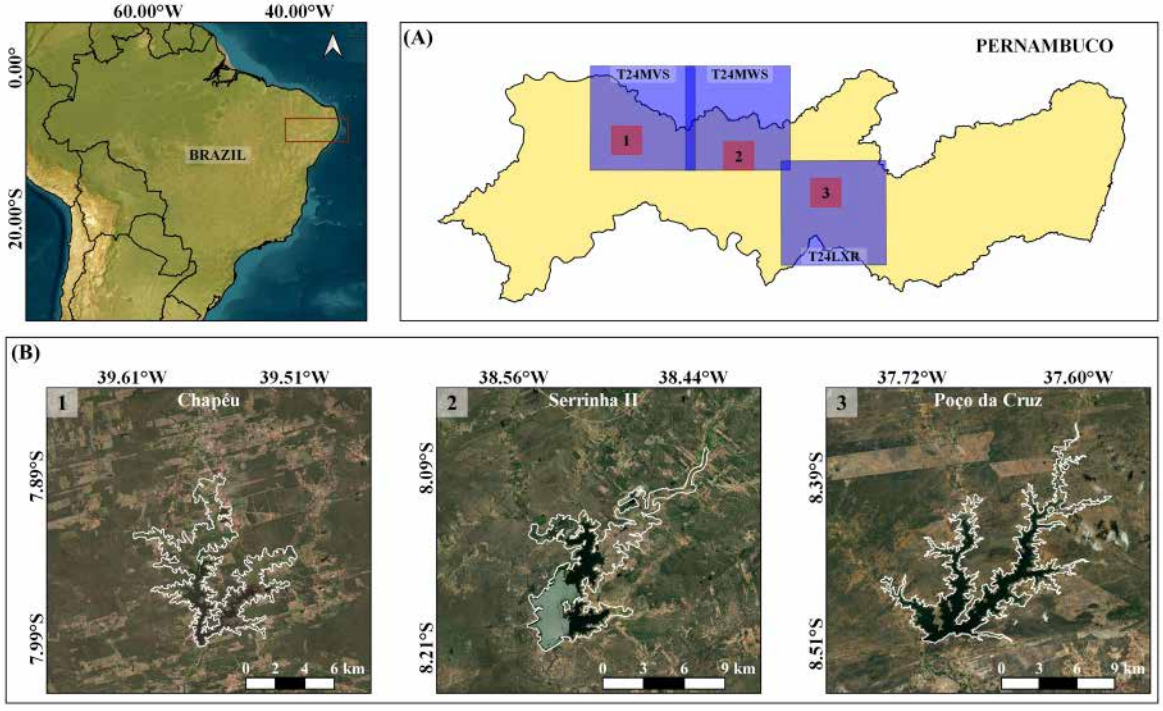

Figure 1 – Location of the selected reservoirs inserted in the Sentinel-2 mission articulation grid with MGRS codes T24MVS, T24MWS, and T24LXR (A). Reservoir contours on an image from the ESRI database (B).

processing methods, eliminating the need for auxiliary data or the creation of temporal series mosaics. Unlike other thresholding approaches that rely on a single dimension, such as a water index, this algorithm combines various water indices and spectral bands into multidimensional hierarchical clusters.

The clustering analysis employed by the algorithm is a technique for identifying similar samples in a multidimensional space. The core idea is to combine water indices with reflectance bands in the visible (VIS), near-infrared (NIR), and shortwave infrared (SWIR) ranges within an automated clustering process. While water indices generally exhibit high values in surface waters, relying on a single index with a threshold can lead to false negatives or positives. Additionally, defining the optimal threshold value can be challenging depending on the scene (Feyisa et al., 2014; Wieland and Martinis, 2019). The algorithm's multidimensional clustering approach addresses this by combining favorable reflectance bands with indices to improve pixel discrimination.

With the algorithm, different combinations using five spectral optical bands and three spectral indices can be made to find the best results for water pixel detection. For this work, the combination of 10 *m* resolution of the MNDWI and NDWI indices with the B12 band in the SWIR (short-wave infrared) spectrum was adopted since, according to Cordeiro et al. (2021), it presented the best balance between robustness and accuracy.

WaterDetect was developed using Python 3.7 and executed on the Linux Ubuntu 20.04 operating system. Sentinel-2 scenes without cloud cover over the reservoirs were selected to generate the water masks.

Statistics for water detection assessment

The water extent values obtained using the methods were compared with monitoring data from *in situ* stations within the ANA network. The evaluation metrics selected were the mean absolute error (MAE, Equation 1), the root mean square error (RMSE, Equation 2), and the relative root mean square error (RRMSE, Equation 3):

$$MAE = \frac{1}{N}\sum_{i=1}^{N}|X_{ref,i} - X_i| \quad (1)$$

$$RMSE = \sqrt{\frac{1}{N}\sum_{i=1}^{N}(X_{ref,i} - X_i)^2} \quad (2)$$

$$RRMSE = 100\sqrt{\frac{1}{N}\frac{\sum_{i=1}^{N}(X_{ref,i} - X_i)^2}{\sum_{i=1}^{N}(X_i)^2}} \quad (3)$$

Where X_{ref} and X are the water area values observed by *in situ* measurements and estimated with satellite products, respectively, and N is the number of days with data.

Bias correction with artificial neural networks

ANNs are characterized by simulation and output processes that enable them to learn the correct response for each input through training. ANNs have been widely utilized for various environmental applications, including precipitation estimation (Tapiador et al., 2004; Pan et al., 2019), hydrological modeling (Wegayehu and Muluneh, 2022; Arsenault et al., 2023), flood forecasting (Dtissibe et al., 2020; Wang, G. et al., 2022), and soil moisture estimation (Han, H. et al., 2021; Singh and Gaurav, 2023). More recently, ANNs have been applied to correct bias in satellite data (Moghim and Bras, 2017; Le et al., 2020; Han, L. et al., 2021; Han, G. et al., 2022). This study used a multilayer perceptron (MLP) regression ANN to correct water surface extents. The rectified linear unit (ReLU) function activated the hidden layers. The ReLU function is beneficial for training deep neural networks as it propagates all positive inputs identically while assigning zero to negative inputs. The weights were optimized using the Adam method, as Kingma and Ba (2017) described it as a stochastic optimizer based on gradients.

The regression MLP ANN was implemented using the SciKit Learn library (Pedregosa et al., 2011) in Python 3. The network consisted of three hidden layers: 150 neurons in the first, 100 in the second, and 50 in the third layer. Different calibration sample sizes within the range (0.1, 0.2, 0.3, 0.4, 0.5) and various values for the maximum number of iterations within the range (200, 205, 210, ···, 400) were tested to determine the model parameters that yielded the best validation results for the MAE, RMSE, and RRMSE metrics (Equations 1, 2, and 3, respectively).

Results and Discussion

Surface Water Extent Using WaterDetect

The WaterDetect algorithm was applied to map water over the three reservoirs considered: Chapéu, Serrinha II, and Poço da Cruz. Despite using a filter to select Sentinel-2 images with less than 20% cloud cover, images with clouds or cloud shadows over the reservoirs were identified and excluded from the result analysis. Additionally, flaws in water masks were detected after processing, resulting in more image exclusion. Table 2 shows the quantity of Sentinel-2 products obtained and the number of products effectively used in the analysis.

The evaluation metrics presented in Equations 1, 2, and 3 were used to assess the quality of water detection by the algorithm and MapBiomas compared to the *in situ* monitoring reference set, as shown in Table 3. The metric values obtained showed significant differences from the *in situ* data. The Poço da Cruz reservoir achieved the best metric results, while the Chapéu reservoir had the lowest performance. However, when comparing the metrics obtained by MapBiomas to the

Table 2 – Quantity of Sentinel-2 products obtained and used in the analysis period.

Reservoir	Sentinel-2 grid	Obtained products	Used products
Chapéu	T24MVS	120	74
Serrinha II	T24MWS	352	170
Poço da Cruz	T24LXR	146	111

in situ monitoring values, all three reservoirs demonstrated lower performance than the metrics achieved by WaterDetect.

Figure 2 presents the observed, calculated, and obtained water area graphs from WaterDetect and MapBiomas. It is important to note that the comparison was made monthly, as MapBiomas generates data only at monthly and annual intervals. A visual analysis of the graphs reveals a considerable difference between the water area values obtained by the algorithm and those from *in situ* observations. However, the calculated values still reflected the dynamics of water area increase and decrease, with the Poço da Cruz reservoir (Figure 2C) standing out. On the contrary, the values obtained by the algorithm and those from MapBiomas show considerable similarity, which may indicate detection issues for both WaterDetect and the MapBiomas methodology, given the underestimation of water area compared to *in situ* values. This underestimation could be attributed to factors such as vegetation cover and shadow at the reservoir edges, which are known to affect water detection algorithms (Yang et al., 2020; Peña-Luque et al., 2021). In the NEB, similar issues have been identified in other studies using optical images, the ISODATA classification method (Moura et al., 2022), and the maximum likelihood method (Lopes and Araújo, 2019).

Water detection quality

To verify the quality of water pixel detection by WaterDetect, the generated water masks were analyzed and compared with the RGB composition and the observed water area values. For instance, Figure 3 presents cases of classification errors for water pixels in each reservoir. Since water in optical sensors is detected by receiving reflected sunlight, detection issues may arise due to cloud cover, shadows, and the direction of the reflected sunlight the satellite sensor receives (Harmel and Chami, 2013). Although there was no cloud cover on the dates corresponding to each reservoir in the cases presented in Figure 3, errors are evident in the composition of the water mask, with "water" pixels being misclassified as "non-water" pixels.

Detection errors such as these can cause significant discrepancies between the calculated water values and those from *in situ* monitoring, as shown in Table 4. The results found in this study using Sentinel-2 products with the WaterDetect algorithm differ from those obtained by Cordeiro et al. (2021), as the authors reported good water detection results with the algorithm, especially in large reservoirs. Additionally, Cordeiro et al. (2021) did not mention pixel classification errors like those observed in the examples presented in Figure 3.

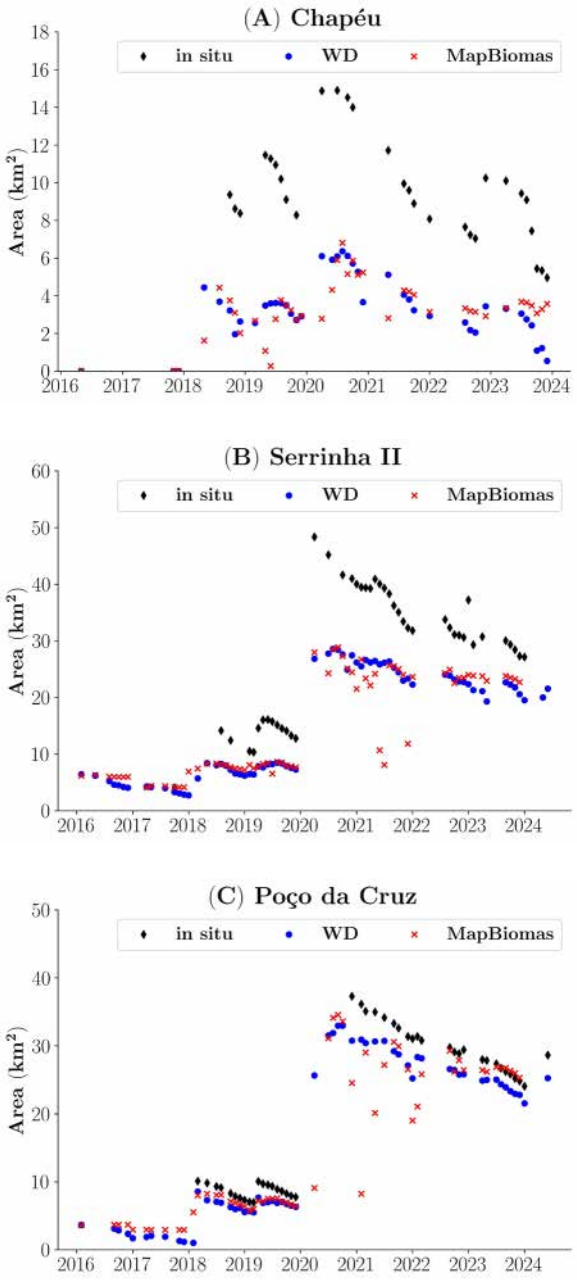

WD: WaterDetect.

Figure 2 – Water area obtained by in situ observations, MapBiomas, and WaterDetect.

Table 3 – WaterDetect and MapBiomas evaluation metrics compared to *in situ* data.

Reservoir	WD × *in situ*			MB × *in situ*		
	MAE[a]	RMSE[a]	RRMSE[b]	MAE	RMSE	RRMSE
Chapéu	6.41	6.53	25.34	6.22	6.72	35.06
Serrinha II	9.33	10.01	4.98	10.46	12.43	9.69
Poço da Cruz	2.93	3.24	1.63	3.52	6.24	4.90

WD: WaterDetect; MB: MapBiomas; MAE: Mean absolute error; RMSE: Root mean square error; RRMSE: Relative root mean square error; [a]Measured in km²; [b]Measured in %.

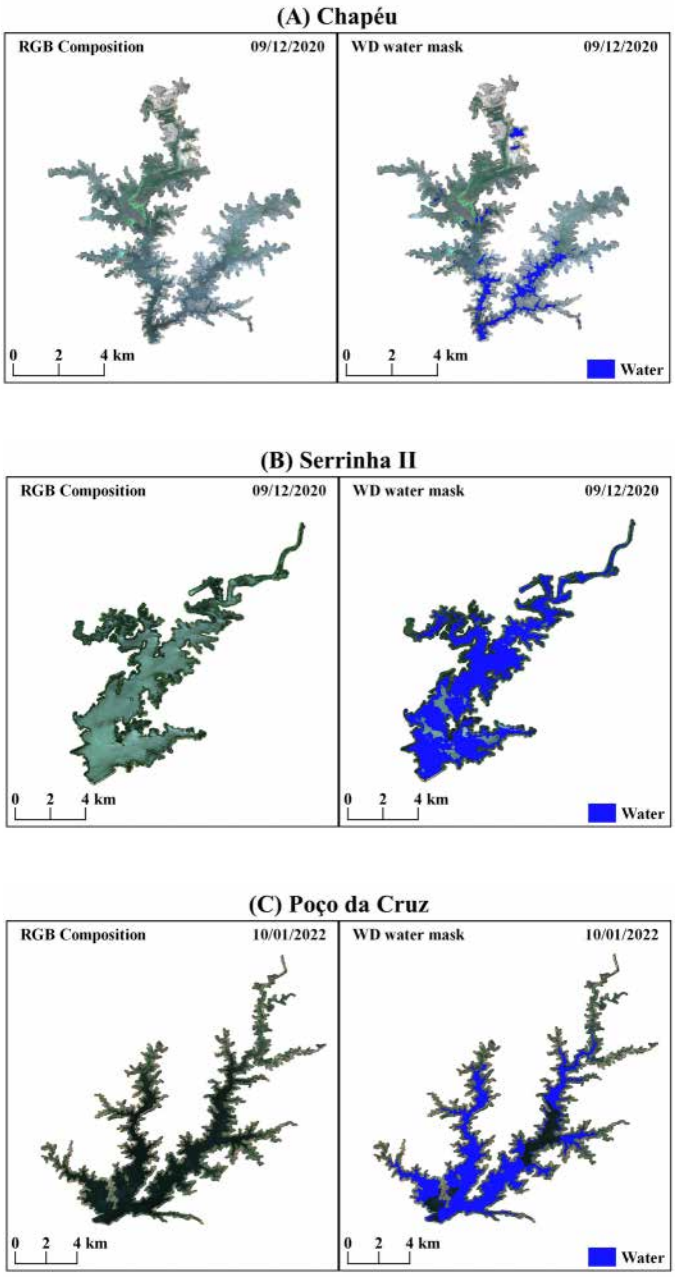

Figure 3 – RGB composition of Sentinel-2 images and water pixels detected by WaterDetect, exemplifying detection errors

On the contrary, Tayer et al. (2023) demonstrated that the default configuration of the WaterDetect algorithm (used in our study) exhibits considerable variability in its water surface detection capability. Figure 4 shows the water occurrence maps obtained from water masks using WaterDetect with Sentinel-2 images. It is noticeable that the three reservoirs have complex shapes with various branches and narrow arms. Additionally, there may be vegetation along the banks of the water bodies. All these factors, along with the pixel mentioned above classification issues, can affect the quality of water detection and, consequently, the surface water area values, even in large reservoirs such as those analyzed in this study (Li et al., 2021; Peña-Luque et al., 2021).

Bias correction of calculated data

The MLP-type ANN was applied to the area values obtained from WaterDetect for bias correction. The results showed that the sample size required for model calibration was equivalent to 20% of the time series for the three reservoirs considered. Calibration sample points were selected randomly to ensure the best possible representation of the time series in the model construction. Table 5 presents the calibration and validation evaluation metrics associated with each reservoir. It can be observed that, regarding the calibration phase of the ANNs,

Table 4 – Examples of images with detection errors impair comparing obtained area values (WaterDetect and *in situ* observations).

Reservoir	Area (km²)		
	WD	in situ	Date
Chapéu	2,566	12,780	09 Dec 2020
Serrinha II	25,905	41,483	09 Dec 2020
Poço da Cruz	22,609	31,063	10 Jan 2022

WD: WaterDetect.

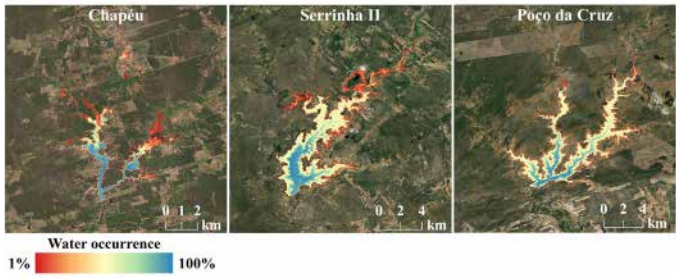

Figure 4 –Water occurrence maps obtained from Sentinel-2 images processed with WaterDetect.

Table 5 – Evaluation metrics applied to bias correction of water surface extension using Artificial Neural Network.

Reservoir	MAE (km²)		RMSE (km²)		RRMSE (%)	
	Cal	Val	Cal	Val	Cal	Val
Chapéu	0,4575	0,8928	0,5432	1,0457	1,06	1,52
Serrinha II	1,5780	2,5153	1,9241	3,3712	1,00	1,22
Poço da Cruz	0,4988	2,8737	0,6401	3,4003	0,44	1,71

MAE: Mean absolute error; RMSE: Root mean square error; RRMSE: Relative root mean square error.

the Poço da Cruz reservoir achieved the best results, followed by the Chapéu reservoir, with Serrinha II showing the poorest results. The metrics presented in Table 5 refer to the calibration and validation stages of the ANN model, so the metric values achieved during validation may not reflect the same precision as those achieved during calibration (Moghim and Bras, 2017).

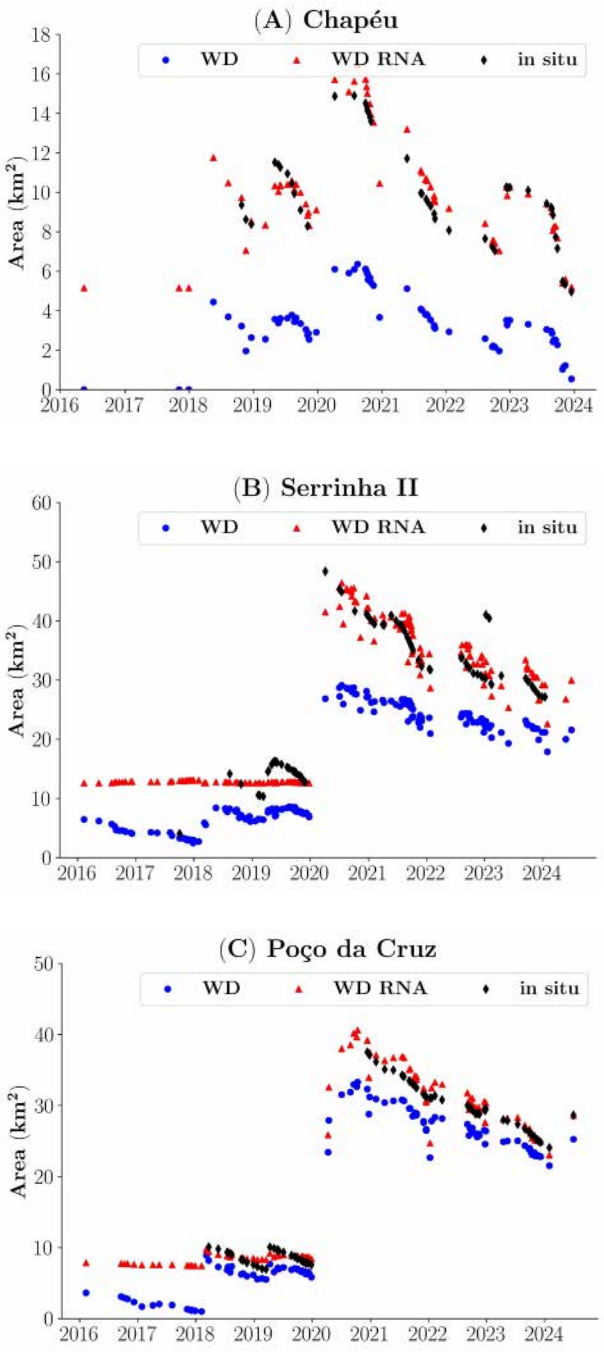

Figure 5 – Observed, calculated, and bias-corrected water area using Sentinel-2 products.

Figure 5 shows the water area values with bias corrected by the MLP ANN. Noticeably, the corrected bias values fit the reference (*in situ*) values for the Chapéu reservoir (Figure 5A). On the contrary, the time series resulting from bias correction for the Serrinha II and Poço da Cruz reservoirs (Figures 5B and 5C, respectively) exhibited two distinct behaviors. The first behavior, identified between 2016 and 2019, shows the poor and unrepresentative adjustment of the corrected values compared to the observed time series. The second behavior, identified between 2020 and 2024, shows that the corrected values fit well for Serrinha II. Poço da Cruz reflects a trend of underestimating the *in situ* values. The disordered behavior presented by the ANN model may be due to an unbalanced selection for the calibration sample used for model calibration, as the *in situ* time series for the Serrinha and Poço da Cruz reservoirs contain a higher number of values above 25 and 30 km², respectively. Factors influencing the accuracy of bias correction using an ANN model include the extent of the time series and the representativeness of the calibration sample used for calibration relative to the reference time series (Han et al., 2022).

Conclusions

The WaterDetect algorithm efficiently identified the water mask in cases without restrictions (clouds or classification errors). However, some difficulties were noted when using optical products from the Sentinel-2 satellite. The first difficulty pertains to the limitation regarding cloud occurrence in the images, such that many products obtained during the analysis period were discarded even in reservoirs located in areas with reduced cloud cover, such as the Sertão region in Pernambuco. Additionally, several water masks generated were excluded from the historical water extent series due to flaws in detecting water pixels. This may indicate a limitation of the algorithm in classifying pixels under specific conditions of sunlight reflection from the water body. The results obtained from WaterDetect and MapBiomas showed considerable similarity, further supporting the hypothesis that using optical images for monitoring reservoirs in the region has limitations.

Two observations can be made from the MapBiomas database. First, MapBiomas's temporal scale is limited, as it provides area values only on a monthly and annual basis, not on a daily scale. Additionally, MapBiomas exhibited a more pronounced underestimation of surface area values, which did not adequately reflect the trend of the historical series.

Finally, the bias correction results using an ANN were generally satisfactory when the calibration sample size and representativeness—specifically, the quantity and balanced distribution of *in situ* monitoring values—were sufficient for constructing the MLP model. In such cases, the same model can be applied to newly calculated water area values, as it efficiently reflects the behavior of the observed historical series.

Authors' Contributions

Souza, J.F.S.: conceptualization, data curation, formal analysis, investigation, methodology, writing – original draft, writing – review & editing. **Ribeiro Neto**, A.: conceptualization, formal analysis, methodology, writing – original draft, writing – review & editing. **Peña-Luque**, S.: conceptualization, investigation, methodology. **Gosset**, M.: conceptualization, investigation, methodology.

References

Arsenault, R.; Martel, J.-L.; Brunet, F.; Brissette, F.; Mai, J., 2023. Continuous streamflow prediction in ungauged basins: long short-term memory neural networks clearly outperform traditional hydrological models. Hydrology and Earth System Sciences, v. 27, 139-157. https://doi.org/10.5194/hess-27-139-2023.

Bai, Z.G.; Dent, D.L.; Olsson, L.; Schaepman, M.E., 2008. Proxy global assessment of land degradation. Soil Use and Management, v. 24, 223-234. https://doi.org/10.1111/j.1475-2743.2008.00169.x.

Chawla, I.; Karthikeyan, L.; Mishra, A.K., 2020. A review of remote sensing applications for water security: quantity, quality, and extremes. Journal of Hydrology, v. 585, 124826. https://doi.org/10.1016/j.jhydrol.2020.124826.

Collischonn, B.; Clarke, R.T., 2016. Estimativa e incerteza de curvas cota-volume por meio de sensoriamento remoto. Revista Brasileira de Recursos Hídricos, v. 21 (4), 719-727. https://doi.org/10.1590/2318-0331.011616022.

Condeça, J.; Nascimento, J.; Barreiras, N., 2022. Monitoring the storage volume of water reservoirs using Google Earth Engine. Water Resources Research, v. 58 (e2021WR030026). https://doi.org/10.1029/2021WR030026.

Cordeiro, M.C.; Martinez, J.-M.; Peña-Luque, S., 2021. Automatic water detection from multidimensional hierarchical clustering for Sentinel-2 images and a comparison with level 2A processors. Remote Sensing of Environment, v. 253, 112209. https://doi.org/10.1016/j.rse.2020.112209.

Drusch, M.; Del Bello, U.; Carlier, S.; Colin, O.; Fernandez, V.; Gascon, F.; Hoersch, B.; Isola, C.; Laberinti, P.; Martimort, P.; Meygret, A.; Spoto, F.; Sy, O.; Marchese, F.; Bargellini, P., 2012. Sentinel-2: ESA's optical high-resolution mission for GMES operational services. Remote Sensing of Environment, v. 120, 25-36. https://doi.org/10.1016/j.rse.2011.11.026.

Dtissibe, F.Y.; Ari, A.A.A.; Titouna, C.; Thiare, O.; Gueroui, A.M., 2020. Flood forecasting based on an artificial neural network scheme. Natural Hazards, v. 104, 1211-1237. https://doi.org/10.1007/s11069-020-04211-5.

Estado de Pernambuco. Plano Estadual de Mudanças Climáticas. Estado de Pernambuco, Recife, 2011, 94 p.

Feyisa, G.L.; Henrik Meilby, H.; Fensholt, R.; Proud, S.R., 2014. Automated water extraction index: a new technique for surface water mapping using Landsat imagery. Remote Sensing of Environment, v. 140, 23-35. https://doi.org/10.1016/j.rse.2013.08.029.

Filippucci, P.; Brocca, L.; Bonafoni, S.; Saltalippi, C.; Wagner, W.; Tarpanelli, A., 2022. Sentinel-2 high-resolution data for river discharge monitoring. Remote Sensing of Environment, v. 281. https://doi.org/10.1016/j.rse.2022.113255.

Han, G.; Zhou, J.; Shao, Q.; Li, W.; Li, C.; Wu, X.; Cao, L.; Wu, H.; Li, Y.; Zhou, G., 2022. Bias correction of sea surface temperature retrospective forecasts in the South China Sea. Acta Oceanologica Sinica, v. 41 (2), 41-50. https://doi.org/10.1007/s13131-021-1880-5.

Han, H.; Choi, C.; Kim, J.; Morrison, R.R.; Jung, J.; Kim, H.S., 2021. Multiple-depth soil moisture estimates using artificial neural network and long short-term memory models. Water, v. 13, 2584. https://doi.org/10.3390/w13182584.

Han, L.; Chen, M.; Chen, K.; Chen, H.; Zhang, Y.; Lu, B.; Song, L.; Qin, R., 2021. A Deep Learning method for bias correction of ECMWF 24-240 h forecasts. Advances in Atmospheric Sciences, v. 38 (9), 1444-1459. https://doi.org/10.1007/s00376-021-0215-y.

Harmel, T.; Chami, M., 2013. Estimation of the sunglint radiance field from optical satellite imagery over open ocean: multidirectional approach and polarization aspects, Journal of Geophysical Research: Oceans, v. 118, 76-90. https://doi.org/10.1029/2012JC008221.

Huang, C.; Chen, Y.; Zhang, S.; Wu, J., 2018. Detecting, extracting, and monitoring surface water from space using optical sensors: A review. Reviews of Geophysics, v. 56 (2), 333-360. https://doi.org/10.1029/2018RG000598.

Jardim, A.M.R.F.; Araújo Júnior, G.N.; Silva, M.V.; Santos, A. Silva, J.L.B.; Pandorfi, H.; Oliveira-Júnior, J.F.; Teixeira, A.H.C.; Teodoro, P.E.; de Lima, J.L.M.P.; Silva Junior, C.A.; Souza, Luciana S.; Silva, Emanuel A.; Silva, Thieres G., 2022. Using remote sensing to quantify the joint effects of climate and land use/land cover changes on the Caatinga Biome of Northeast Brazilian. Remote Sensing, v. 14, 1911. https://doi.org/10.3390/rs14081911.

Kingma, D.P.; Ba, J.A., 2017. A method for stochastic optimization. arXiv, 1412.6980. https://doi.org/10.48550/arXiv.1412.6980.

Lasko, K.; Maloney, M.C.; Becker, S.J.; Griffin, A.W.H.; Lyon, S.L.; Griffin, S.P., 2021. Automated training data generation from spectral indexes for mapping surface water extent with sentinel-2 satellite imagery at 10 m and 20 m resolutions. Remote Sensing, v. 13, 4531. https://doi.org/10.3390/rs13224531

Le, X.; Lee, G.; Jung, K.; An, H.; Lee, S.; Jung, Y., 2020. Application of convolutional neural network for spatiotemporal bias correction of daily satellite-based precipitation. Remote Sensing, v. 12 (17), 2731. https://doi.org/10.3390/rs12172731.

Li, J.; Ma, R.; Cao, Z.; Xue, K.; Xiong, J.; Hu, M.; Feng, X., 2022. Satellite detection of surface water extent: A review of methodology. Water, v. 14 (7). https://doi.org/10.3390/w14071148.

Li, J.; Peng, B.; Wei, Y.; Ye, H., 2021. Accurate extraction of surface water in complex environment based on Google Earth Engine and Sentinel-2. PLoS ONE, v. 16 (6), e0253209. https://doi.org/10.1371/journal.pone.0253209.

Lopes, J.W.B.; Araújo, J.C., 2019. Simplified method for the assessment of siltation in semiarid reservoirs using satellite imagery. Water, v. 11, 1-18. https://doi.org/10.3390/w11050998.

Marengo, J.A.; Galdos, M.V.; Challinor, A.; Cunha, A.P.; Marin, F.R.; Vianna, M.d.S.; Alvala, R.C.S.; Alves, L.M.; Moraes, O.L.; Bender, F., 2022. Drought in Northeast Brazil: A review of agricultural and policy adaptation options for food security. Climate Resilience and Sustainability, v. 1, e17. https://doi.org/10.1002/cli2.17.

Marengo, J.A.; Torres, R.R.; Alves, L.M., 2017. Drought in Northeast Brazil-past, present, and future. Theoretical and Applied Climatology, v. 129, 1189-1200. https://doi.org/10.1007/s00704-016-1840-8.

McFeeters, S.K.; 1996. The use of the normalized difference water index (NDWI) in the delineation of open water features. International

Journal of Remote Sensing, v. 17 (7), 1425-1432. https://doi.org/10.1080/01431169608948714.

Moghim, S.; Bras, R.L., 2017. Bias correction of climate modeled temperature and precipitation using artificial neural networks. Journal of Hydrometeorology, American Meteorological Society, v. 18 (7), 1867-1884. https://doi.org/10.1175/JHM-D-16-0247.1.

Moura, M.P.; Ribeiro Neto, A.; Costa, F.A. 2022. Application of satellite imagery to update depth-area-volume relationships in reservoirs in the semiarid region of Northeast Brazil. Revista Brasileira de Engenharia Agrícola e Ambiental, v. 26, 44-50. https://doi.org/10.1590/1807-1929/agriambi.v26n1p44-50.

Mueller-Wilm, U.; Devignot, O.; Pessiot, L. Sen2Cor configuration and user manual. Telespazio VEGA Deutschland GmbH: Darmstadt, Germany, 2016 (Accessed July 15, 2024) at:. https://step.esa.int/thirdparties/sen2cor/2.11.0/docs/OMPC.TPZG.SUM.001%20-%20i1r0%20-%20Sen2Cor%202.11.00%20Configuration%20and%20User%20Manual.pdf.

Otsu, N., 1979. A threshold selection method from gray-level histograms. IEEE Transactions on Systems, Man, and Cybernetics, v. 9 (1), 62-66. https://doi.org/10.1109/TSMC.1979.4310076.

Pan, B.; Hsu, K.; AghaKouchak, A.; Sorooshian, S., 2019. Improving precipitation estimation using Convolutional Neural Network. Water Resources Research, v. 55 (3), 2301-2321. https://doi.org/10.1029/2018WR024090.

Pedregosa, F.; Varoquaux, G.; Gramfort, A.; Michel, V.; Thirion, B., 2011. Scikit-learn: Machine Learning in Python. Journal of Machine Learning Research, v. 12, 2825-2830 (Accessed July 15, 2024) at:. http://jmlr.org/papers/v12/pedregosa11a.html

Peña-Luque, S.; Ferrant, S.; Cordeiro, M.C.R.; Ledauphin, T.; Maxant, J.; Martinez, J-M., 2021. Sentinel-1&2 multitemporal water surface detection accuracies, evaluated at regional and reservoirs level. Remote Sensing, v. 13 (16), 3279. https://doi.org/10.3390/rs13163279.

Reis, L.G.M.; Souza, W.O.; Ribeiro Neto, A.; Fragoso Jr., C.R.; Ruiz-Armenteros, A.M.; Cabral, J.J.S.P.; Montenegro, S.M.G.L., 2021. Uncertainties involved in the use of thresholds for the detection of water bodies in multitemporal analysis from Landsat-8 and Sentinel-2 images. Sensors, v. 21 (22), 7494. https://doi.org/10.3390/s21227494.

Secretaria de Infraestrutura e Recursos Hídricos de Pernambuco (SEINFRA-PE), 2022. Plano Estadual de Recursos Hídricos de Pernambuco — PERH/PE. v. 4 — Diagnóstico Integrado. Secretaria de Infraestrutura e Recursos Hídricos de Pernambuco, Recife, 299 p (Accessed July 15, 2024) at:. https://www.apac.pe.gov.br/planos.

Singh, A.; Gaurav, K., 2023. Deep learning and data fusion to estimate surface soil moisture from multi-sensor satellite images. Scientific Reports, v. 13, 2251. https://doi.org/10.1038/s41598-023-28939-9.

Sistema de Estimativas de Emissões de Gases de Efeito Estufa do Observatório do Clima (SEEG/OC). Projeto MapBiomas - Coleção 8 da Serie Anual de Mapas de Uso e Cobertura da Terra do Brasil. Brasília, 2022 (Accessed September 21, 2023) at:. https://brasil.mapbiomas.org/map/colecao-8/

Souza, C.M.; Shimbo, J.; Rosa, M.R.; Parente, L.L.; Alencar, A.; Rudorff, B.F.T.; Hasenack, H.; Matsumoto, M.; Ferreira, L.; Souza-Filho, P.W.M.; Oliveira, S.W.; Rocha, W.F.; Fonseca, A.V.; Marques, C.B.; Diniz, C.G.; Costa, D.; Monteiro, D.; Rosa, E.R.; Vélez-Martin, E.; Weber, E.J.; Lenti, F.E.B.; Paternost, F.F.; Pareyn, F.G.C.; Siqueira, J.V.; Viera, J.L.; Neto, L.C.F.; Saraiva, M.M.; Sales, M.H.; Salgado, M.P.G.; Vasconcelos, R.; Galano, S.; Mesquita, V.V.; Azevedo, T., 2020. Reconstructing three decades of land use and land cover changes in Brazilian Biomes with Landsat archive and Earth Engine. Remote Sensing, v. 12 (17). https://doi.org/10.3390/rs12172735.

Tapiador, F.J.; Kidd, C.; Hsu, K.-L.; Marzano, F., 2004. Neural networks in satellite rainfall estimation. Meteorological Applications, v. 11 (1), 83-91. https://doi.org/10.1017/S1350482704001173.

Tayer, T.C.; Douglas, M.M.; Cordeiro, M.C.R.; Tayer, A.D.N.; Callow, J.N.; Beesley, L.; McFarlane, D., 2023. Improving the accuracy of the Water Detect algorithm using Sentinel-2, Planetscope and sharpened imagery: a case study in an intermittent river. GIScience & Remote Sensing, v. 60 (1), 2168676. https://doi.org/10.1080/15481603.2023.2168676.

United Nations. Sustainable Development Goal 6 Synthesis Report 2018 on Water and Sanitation. United Nations, New York, 2018, 195 p.

Wang, G.; Yang, J.; Hu, Y.; Li, J.; Yin, Z., 2022. Application of a novel artificial neural network model in flood forecasting. Environmental Monitoring and Assessment, v. 194 (125). https://doi.org/10.1007/s10661-022-09752-9.

Wang, X.; Xie, S.; Zhang, X.; Chen, C.; Guo, H.; Du, J.; Duan, Z., 2018. A robust Multi-Band Water Index (MBWI) for automated extraction of surface water from Landsat 8 OLI imagery. International Journal of Applied Earth Observation and Geoinformation, v. 68, 73-91. https://doi.org/10.1016/j.jag.2018.01.018.

Wegayehu, E.B.; Muluneh, F.B., 2022. Short-term daily univariate streamflow forecasting using deep learning models. Advances in Meteorology, e1860460. https://doi.org/10.1155/2022/1860460.

Wieland, M.; Martinis, S., 2019. A modular processing chain for automated flood monitoring from multispectral satellite data. Remote Sensing, v. 11 (19). https://doi.org/10.3390/rs11192330.

Wieland, M.; Martinis, S., 2020. Large-scale surface water change observed by Sentinel-2 during the 2018 drought in Germany. International Journal of Remote Sensing, v. 41 (12), 4742-4756. https://doi.org/10.1080/01431161.2020.1723817.

Xu, H., 2006. Modification of normalized difference water index (NDWI) to enhance open water features in remotely sensed imagery. International Journal of Remote Sensing, v. 27 (14), 3025-3033. https://doi.org/10.1080/01431160600589179.

Yang, X.; Qin, Q.; Yésou, H.; Ledauphin, T.; Koehl, M.; Grussenmeyer, P.; Zhu, Z., 2020. Monthly estimation of the surface water extent in France at a 10-m resolution using Sentinel-2 data. Remote Sensing of Environment, v. 244, 111803. https://doi.org/10.1016/j.rse.2020.111803.

Yilmaz, O.S.; Gulgen, F.; Balik Sanli, F.; Ates, A.M., 2023. The performance analysis of different water indices and algorithms using Sentinel-2 and Landsat-8 images in determining water surface: Demirkopru Dam case study. Arabian Journal for Science and Engineering, v. 48, 7883-7903. https://doi.org/10.1007/s13369-022-07583-x.